

Received March 13, 2021, accepted June 2, 2021, date of publication June 21, 2021, date of current version June 30, 2021.

Digital Object Identifier 10.1109/ACCESS.2021.3091307

Multi-Granularity Genetic Programming Optimization Method for Satellite System Topology and Parameter

JINHUI LI¹ AND YUNFENG DONG²

¹School of Astronautics, Beihang University, Beijing 100191, China

²Key Laboratory of Spacecraft Design Optimization and Dynamic Simulation Technologies, Ministry of Education, Beijing 100191, China

Corresponding author: Jinhui Li (lijinhui1990@buaa.edu.cn)

This work was supported in part by the National Key Research and Development Program of China under Grant 2016YFB0501102, and in part by the Key Laboratory of Spacecraft Design Optimization and Dynamic Simulation Technologies, Ministry of Education.

ABSTRACT Granular computing is usually considered as a representative method for solving complex problems, which can be solved quickly through freely switching among different granular models. In this paper, a genetic programming method based on the concept of granular computing is proposed to provide an efficient solution for optimizing the topology and parameters of a satellite system simultaneously. According to the coupling relationship of multiple physical fields, the multi-granularity description method of the satellite system scheme is defined and a multi-granularity digital satellite model is constructed. The genetic programming method is improved according to the principle of falsity preserving in granular computing. The concept and calculation method of granular risk factor are proposed to allow different individuals of the current population to switch among different granularities. The convergence difficulty caused by the complexity, hugeness, and high integration of satellites is effectively alleviated. The application to design and optimize an earth observation satellite proves the effectiveness of the proposed method.

INDEX TERMS Satellite system design, system topology optimization, granular computing, genetic programming, MBS.

I. INTRODUCTION

System engineering is the theoretical basis for satellite system design. Text-based systems engineering (TBSE) has been widely applied in the 1980s. When the spacecraft becomes complex, the application of TBSE shows limitations. In addition to the problems of low cooperation efficiency and long development cycle, the main problem is that the system design scheme cannot be accurately evaluated quantitatively. For instance, one of the important reasons for the accidents of the space shuttle Challenger [1], [2] and Columbia [3] in history is that there is not enough quantitative evaluation in the design stage. Currently, model-based systems engineering (MBSE) is gradually replacing TBSE to apply in complex satellite design. In MBSE, quantitative evaluations are usually applied to help improve the design scheme of the spacecraft. One of the mature MBSE applications is conducted by NASA, who developed an MBSE infrastructure [4] and

applied it to help design CubeSat [5], James Weber Space Telescope [6], and the MARS 2020 project [7]. However, the above-mentioned applications involve more or less human participation in the design process. We aim to use MBSE for satellite design with autonomous optimization procedure. More specifically, we try to look for a new optimization method and develop a new system modeling method to optimize system topology and parameters simultaneously.

In terms of optimization methods, parameter optimization algorithms and topology optimization algorithms have been studied a lot. However, in the previous study of the satellite system design, almost all of the successful applications are based on parameter optimization algorithms. The most widely used algorithms include genetic algorithm [8], ant colony algorithm [9], and simulated annealing algorithm [10]. However, in the algorithms above, the structures of the optimization objects are invariant. Therefore, these algorithms are not suitable for the optimization of the satellite system composition and structure (i.e., the system topology), which is also very important in satellite system optimization

The associate editor coordinating the review of this manuscript and approving it for publication was Mohamed Elhoseny¹.

besides system parameters. This problem restricts the effectiveness of satellite system design and the optimality of the scheme. One of the promising methods that can optimize system topology and parameters simultaneously is genetic programming (GP) proposed by Professor Koza [11]. GP is widely used in the optimal design of mechatronic systems. Sripramong *et al.* [12] designed an automatic circuit design system for a CMOS amplifier by GP. Sun *et al.* [13] realized the automatic evolution of satellite attitude control law expression by GP. Malhotra *et al.* [14] evolved a threshold comparator circuit of a satellite for safe mode detection by GP. The main feature of these current applications of GP is that the system model is relatively simple and only involves a single discipline. In contrast, the satellite system model is much more complex, including multidisciplinary coupling relationships.

Another key problem when applying MBSE in satellite system design optimization lies in satellite digital modeling. In previous studies, simplified satellite models or empirical formulas are enough for satellite parameters optimization. But for satellite topology optimization, it is necessary to develop a complex model including the coupling relationship of satellite system components and structures. The quantitative evaluation of a single complex model will cost a lot of computing resources. And it will cost much more resources in the process of satellite system design optimization where a large number of satellite schemes are supposed to be quantitatively evaluated and compared. On the other hand, the complex model may also have convergence difficulty during optimization [15]. According to the granular computing theory, the uncertainty of the concept model is closely related to granularity [16]. A human can switch freely among different granularities according to the complexity of the problem. A plan can be assessed under coarse granularity with little resources and time consumption. Once the plan is evaluated and considered applicable, it can then be more detailly evaluated under fine granularity with less uncertainty [17], [18]. For this reason, the satellite design and optimization process can be divided into different stages by designers [19]. In the early stage, some influencing factors are neglected and the coarse granularity model is used for optimization. In the subsequent design stages, fine granularity models are gradually used to obtain more reliable results. The design phase and the model granularity are coupled, thus making the optimization process to be iterative [20]. However, as far as we know, there is little mature application of granular computing theory in satellite system design optimization. Current researches mainly have two limitations: 1) lacking multi-granularity expressions in satellite digital modeling methods, and 2) lacking expressions and processing methods of multi-granularity individuals in GP applications.

In this paper, the idea of granular computing and the GP method is introduced to optimize the system design scheme of a satellite. Genetic programming is used to describe the topology of the satellite system. It breaks through the limitation of the expression of the general parameter optimization

algorithms. The idea of granular computing is introduced into the optimization process. The simple model is used for rough selection, and the complex model is used for fine selection. With relatively low consumption of computing resources, the satellite system topology and parameter optimization problems can be quickly converged.

The main contributions of this paper lie in the following two aspects: 1) By combining the granular computing theory with the satellite digital modeling method, a multi-granular satellite digital model definition method is proposed, which provides the model granularity choice for the satellite system design; 2) A multi-granularity genetic programming optimization (MGGPO) method is proposed and applied to the optimization design of satellite system scheme, which reduces resource consumption and improves efficiency.

The remainder of this paper is organized as follows. Section II introduces the problem description of multi-granularity satellite system design optimization. In Section III, the method of establishing multi-granularity satellite models is described. The MGGPO method is presented in Section IV. Then the flowchart of satellite system design optimization based on MGGPO is shown in Section V. The case study and analysis are given in Section VI. Finally, the conclusions are provided in Section VII.

II. PROBLEM DESCRIPTION OF MULTI-GRANULARITY SATELLITE SYSTEM DESIGN OPTIMIZATION

The optimization problem of the satellite system design can be described as [21]

$$\begin{aligned} & \text{find } \mathbf{S} \\ & \text{min } J(\mathbf{X}) \\ & \text{s.t. } \mathbf{S} \xrightarrow{D_S} f \\ & \quad \dot{\mathbf{X}} = f(\mathbf{X}), \mathbf{X}(t_0) = \mathbf{X}_0 \\ & \quad C(\mathbf{X}) \leq 0 \end{aligned} \quad (1)$$

where \mathbf{S} represents the design variable of the optimization problem, which is a possible satellite system design scheme; f represents the digital model uniquely determined by a specified satellite scheme \mathbf{S} ; D_S represents the digital modeling method, and the mapping relation between \mathbf{S} and f is expressed as $\mathbf{S} \xrightarrow{D_S} f$; \mathbf{X} is the set where all the states of the satellite system described in f are included; t_0 is the initial time, and the \mathbf{X}_0 is the initial value of \mathbf{X} ; $\dot{\mathbf{X}} = f(\mathbf{X})$, $\mathbf{X}(t_0) = \mathbf{X}_0$ express the system state equation of the satellite; $J(\mathbf{X})$ is the objective function of the satellite system design; $C(\mathbf{X})$ is the constraints of the satellite system design. Our purpose is to find a satellite system scheme described by design variables \mathbf{S} to minimize the objective function $J(\mathbf{X})$, e.g., an equivalent index concerning mass and cost, under constraints $C(\mathbf{X})$.

According to the theory of granular computing [22], an equivalence relation of scheme \mathbf{S} is defined on a coarse granularity. The quotient set of \mathbf{S} can be obtained, which is denoted as $[\mathbf{S}]$. Similarly, we can get the quotient set $[f]$, $[\mathbf{X}]$, $[J]$, and $[C]$, corresponding to f , \mathbf{X} , J , and C respectively.

Denoting the original optimization problem as $(\mathbf{S}, f, \mathbf{X}, J, C)$, the quotient space on a certain granularity can be expressed as $([\mathbf{S}], [f], [\mathbf{X}], [J], [C])$. When we study the same problem using different granularity, we can get the results of different granularity, such as $([\mathbf{S}]_1, [f]_1, [\mathbf{X}]_1, [J]_1, [C]_1)$, $([\mathbf{S}]_2, [f]_2, [\mathbf{X}]_2, [J]_2, [C]_2)$.

In this paper, three kinds of granularity of the satellite model are defined. The coarsest granularity is called the point satellite model (short for point model), and its quotient space is defined as $([\mathbf{S}]_p, [f]_p, [\mathbf{X}]_p, [J]_p, [C]_p)$. In the point model, it is assumed that each satellite service subsystem is ideal and can work perfectly without affecting the system function. In the point satellite model, the satellite orbit motion is the main concern. The second level of granularity is called the stream satellite model (short for stream model), and its quotient space is defined as $([\mathbf{S}]_s, [f]_s, [\mathbf{X}]_s, [J]_s, [C]_s)$. In the stream satellite model, it is assumed that the satellite subsystems do not affect each other, each component is an ideal component, and it will not affect other components except those involved in the stream of its function. The finest granularity is called the field satellite model (short for field model), and its quotient space is defined as $([\mathbf{S}]_f, [f]_f, [\mathbf{X}]_f, [J]_f, [C]_f)$. Some characteristics of the digital twin system are included in the field satellite model, that is, multi-dynamic, multi-scale, and multi-physical field coupling. Multi-dynamic refers to the orbit, attitude, and micro-vibration spectrum. Multi-scale includes celestial bodies, whole satellite, and components. Multi-physical fields mainly include mechanical, electrical, thermal, optical, magnetic, and radiation fields.

The principle of falsity preserving quotient space points out that if there is no solution to a problem in the quotient space, there must be no solution to the corresponding problem in the original space [22]. For the satellite system design optimization problem, the three granularities defined in the previous paragraph are introduced, and the design variable \mathbf{S} becomes a set of schemes with multiple granularities. The objective function becomes to find the minimum J in the finest granularity. Constraints are determined from the point model, stream model, and field model, and can be satisfied under each granularity. The problem of multi-granularity satellite system design optimization can be described as follows

$$\begin{aligned}
 & \text{find } \mathbf{S} = \{[\mathbf{S}]_p, [\mathbf{S}]_s, [\mathbf{S}]_f\} \\
 & \text{min } [J]_f([\mathbf{X}]_f) \\
 & \text{s.t. } [\mathbf{S}]_p \xrightarrow{D_s} [f]_p \\
 & \quad [\dot{\mathbf{X}}]_p = [f]_p([\mathbf{X}]_p), [\mathbf{X}]_p(t_0) = [\mathbf{X}_0]_p \\
 & \quad [C]_p([\mathbf{X}]_p) \leq 0 \\
 & \quad [\mathbf{S}]_s \xrightarrow{D_s} [f]_s \\
 & \quad [\dot{\mathbf{X}}]_s = [f]_s([\mathbf{X}]_s), [\mathbf{X}]_s(t_0) = [\mathbf{X}_0]_s \\
 & \quad [C]_s([\mathbf{X}]_s) \leq 0 \\
 & \quad [\mathbf{S}]_f \xrightarrow{D_s} [f]_f \\
 & \quad [\dot{\mathbf{X}}]_f = [f]_f([\mathbf{X}]_f), [\mathbf{X}]_f(t_0) = [\mathbf{X}_0]_f \\
 & \quad [C]_f([\mathbf{X}]_f) \leq 0
 \end{aligned} \tag{2}$$

where $[\mathbf{X}_0]_p$, $[\mathbf{X}_0]_s$, and $[\mathbf{X}_0]_f$ represent the initial values of $[\mathbf{X}]_p$, $[\mathbf{X}]_s$, and $[\mathbf{X}]_f$, respectively. The objective function and constraints of the field model are defined in our previous work [21]. Two levels of the index system are established which are the system indices and subsystem indices. The system indices include mass, cost, reliability, cost-effectiveness ratio, and performance. Indices of the payload subsystem include the total power consumption of itself, data rate, ground sample distance, ground coverage half center angle, total information transmission, coverage performance of target, coverage bandwidth, signal to noise ratio of the image. Indices of the attitude determination & control subsystem (ADCS) subsystem include attitude measurement accuracy, attitude direction accuracy, attitude stability accuracy, attitude maneuver angular velocity, stability time after maneuvering, orbit control accuracy, orbit control acceleration, flywheel control torque. Indices of the power subsystem include the total power consumption of itself, mass to power ratio, solar wing orientation accuracy, solar array power margin, output power at the beginning of life, output power at the end of life, battery capacity, discharge depth, average eclipse factor. Indices of the propulsion subsystem include propellant mass, specific impulse, propellant extrusion efficiency, total impulse. Indices of the TT&C subsystem include total power consumption of itself, data transmission rate, ground station TT&C coverage performance, the quality of the TT&C receiving system (GT), equivalent isotropically radiated power (EIRP). Indices of the thermal subsystem include the total power consumption of itself, minimum and maximum temperatures of typical components, the equilibrium temperature of the satellite, the minimum and maximum temperature of the satellite in the orbital period. Indices of the structure subsystem include the structural strength, axial frequency, transverse frequency, envelope diameter, envelope height, body width, the diameter of the bearing cylinder, satellite volume, the ultimate stress required by strength, the critical stress required by stability.

For the stream model, the objective function and constraints are the same as those of the field model. For the point model, the objective function and constraints are almost the same as those of the field model, except for a few indices that are not available under the point model. These indices that are not included in the point model include flywheel control torque, minimum and maximum temperatures of typical components.

The definition of the multi-granularity satellite model $[f]_p([\mathbf{X}]_p)$, $[f]_s([\mathbf{X}]_s)$, $[f]_f([\mathbf{X}]_f)$ is given in Section III. The multi-granularity tree structure expression $\{[\mathbf{S}]_p, [\mathbf{S}]_s, [\mathbf{S}]_f\}$ and genetic programming method are given in Section IV.

III. MULTI-GRANULARITY MODELS OF SATELLITE

The satellite system model provides support for the quantitative evaluation of satellite schemes. To find out the real impact of the changes of system topology on the optimization objectives, it is necessary to establish a satellite model as complex as possible. The most complex satellite digital model is

called the field model. The field model has the characteristics of multi-dynamic, multi-scale, and multi-physical field coupling. By neglecting or simplifying the coupling relationship of some dynamic spectrum, spatial scales, and physical field, the stream model and point model are obtained. In the following subsections, the point model, stream model, and field model of ADCS and thermal subsystem will be introduced as examples.

A. POINT MODEL

In the point model, only the celestial body scale and the satellite scale are considered in the multi-scale. The multi-dynamic and multi-physics coupling are not considered.

1) ADCS SUBSYSTEM POINT MODEL

In the point model, the ADCS subsystem is ideal, in which the characters of various components are no longer important. An ideal sensor and an ideal actuator can be used to replace various personalized component combinations. In the dynamic equation, only the control force and torque generated by the ideal actuator are included. The system state variable set of the ADCS subsystem point model is a subset of the satellite system state $[X]_p$. It consists of variables in orbit dynamics and attitude dynamics. In orbit dynamics, m is the total mass of the satellite, V is the velocity vector of the satellite, F_{out} is the combined external force of the environment, and F_{ideal} is the force of the ideal actuator. In attitude dynamics, I is the total inertia, ω is the attitude angular velocity, M_{out} is the resultant torque of the environment and M_{ideal} is the torque of the ideal actuator [23]. The orbit and attitude dynamic equations of the point model are established as follows

$$\begin{cases} \frac{dV}{dt} = \frac{1}{m} (F_{out} + F_{ideal}) \\ \frac{d\omega}{dt} = I^{-1} (M_{out} + M_{ideal} - \omega \times I\omega) \end{cases} \quad (3)$$

2) THERMAL SUBSYSTEM POINT MODEL

In the point model, each subsystem is ideal, in which the difference in local temperature is no longer important. Assuming that the temperature inside the satellite is the same, the surface of the satellite is coated with multiple layers of heat insulation material, and the heat dissipation surface is not covered with heat insulation material but sprayed with white paint. The thermal network model is built with the satellite interior (T_0), six exterior surfaces (T_1 to T_6), and up to six exterior surfaces (T_7 to T_{12}). The heat balance equation of the exterior surfaces and the heat dissipation windows is as follows

$$C_i \frac{dT_i}{dt} = \alpha_i \bar{q}_{exi} A_i + A_i \lambda_i (T_0 - T_i) \delta_i^{-1} - \varepsilon_i \sigma A_i T_i^4 \quad (i = 1, 2, \dots, 12) \quad (4)$$

where C_i is the heat capacity of node i , ε_i is the emissivity of node i , σ is the Boltzmann constant with a value of $1.38 \times 10^{-23} J/K$, A_i is the area of node i , T_i is the temperature of node i , λ_i is the equivalent thermal conductivity of multilayer

or structural plate, δ_i is the thickness, α_i is the absorptivity of node i , \bar{q}_{exi} is the average external radiation heat flux of each surface [24].

The heat balance equation of node 0 inside the satellite is

$$C_s \frac{dT_0}{dt} = \sum_{i=1}^{12} \frac{A_i \lambda_i (T_i - T_0)}{\delta_i} + P_{thm} \quad (5)$$

where P_{thm} is the heat power consumption in the satellite; C_s is the heat capacity of the satellite [24].

B. STREAM MODEL

In the stream model, the three scales of celestial bodies, satellites, and components are all considered. Multi-dynamic and multi-physics coupling are not considered.

1) ADCS SUBSYSTEM STREAM MODEL

In the stream model, the real function stream of the ADCS subsystem is simulated, and the characteristics of different sensors and actuators are considered. In the dynamic equation, the control force and torque generated by the thrusters and momentum exchange devices are included. The system state variable set of the ADCS subsystem stream model is a subset of the satellite system state $[X]_s$. Compared with the point model, three state variables are added. $F_{thruster}$ is the resultant force of all thrusters, $M_{thruster}$ is the resultant torque of all thrusters, and M_{wheel} is the torque of momentum exchange devices [23]. The orbit and attitude dynamic equations in the stream model are established as follows

$$\begin{cases} \frac{dV}{dt} = \frac{1}{m} (F_{out} + F_{thruster}) \\ \frac{d\omega}{dt} = I^{-1} (M_{out} + M_{thruster} + M_{wheel} - \omega \times I\omega) \end{cases} \quad (6)$$

where the torque formula of momentum exchange device is as follows

$$M_{wheel} = -(\dot{H}_W + \omega \times H_W + \omega_W \times H_W) \quad (7)$$

where H_W and ω_W represent angular momentum and angular velocity of the flywheel in satellite respectively [23].

2) THERMAL SUBSYSTEM STREAM MODEL

In the stream model, each subsystem is relatively independent, and there is no coupling between components, so the temperature difference of different subsystem components is not considered. The heat network model and heat balance equation of the satellite are the same as those in the point model.

C. FIELD MODEL

In the field model, the three spatial scales of celestial bodies, satellites, and components, the three spectrum dynamics of orbit, attitude, and micro-vibration, and the coupling of various physical fields of mechanics, electricity, heat, light, magnetism, and radiation are all considered. The multi-dynamic model in the field model is introduced by taking the ADCS

subsystem model as the first example. The multi-scale and multi-physics coupling model in the field model is introduced by taking the thermal subsystem model as the second example.

1) MULTI-DYNAMIC MODEL

The system state variable set of the ADCS subsystem field model is a subset of the satellite system state $[\mathbf{X}]_f$. Compared with the stream model, several state variables related to large flexible attachments, liquid-filled tanks, and manipulators are added. $\mathbf{F}_{flexible}$, \mathbf{F}_{tank} , \mathbf{F}_{arm} are the forces of flexible attachments, liquid-filled tanks, and manipulators on rigid satellite body respectively. $\mathbf{M}_{flexible}$, \mathbf{M}_{tank} , \mathbf{M}_{arm} are the torques of flexible attachments, liquid-filled tanks, and manipulators on rigid satellite body [23]. The orbit and attitude dynamic equations in the field model are established as follows

$$\begin{cases} \frac{d\mathbf{V}}{dt} = \frac{1}{m} (\mathbf{F}_{out} + \mathbf{F}_{thruster} + \mathbf{F}_{flexible} + \mathbf{F}_{tank} + \mathbf{F}_{arm}) \\ \frac{d\omega}{dt} = \mathbf{I}^{-1} \left(\begin{matrix} \mathbf{M}_{out} + \mathbf{M}_{thruster} + \mathbf{M}_{wheel} + \mathbf{M}_{flexible} \\ + \mathbf{M}_{tank} + \mathbf{M}_{arm} - \omega \times \mathbf{I}\omega \end{matrix} \right) \end{cases} \quad (8)$$

where $\mathbf{F}_{flexible}$ and $\mathbf{M}_{flexible}$ are obtained through the micro-vibration model. They can be calculated as follows

$$\begin{aligned} \mathbf{F}_{flexible} &= - \sum_i \mathbf{B}_{trani} \ddot{\mathbf{q}}_i \\ \mathbf{M}_{flexible} &= - \sum_i \mathbf{B}_{roti} \ddot{\mathbf{Q}}_i \end{aligned} \quad (9)$$

where \mathbf{B}_{trani} and \mathbf{B}_{roti} represent the translational and rotational coupling matrix of the i^{th} flexible attachment, and \mathbf{q}_i represents the modal coordinates of the i^{th} flexible attachment [23]. The translational and rotational coupling matrix can be expressed as

$$\begin{aligned} \underline{\mathbf{B}}_{tran} &= [\mathbf{B}_{tran}^1, \mathbf{B}_{tran}^2, \dots, \mathbf{B}_{tran}^j, \dots, \mathbf{B}_{tran}^l]^T \\ \underline{\mathbf{B}}_{rot} &= [\mathbf{B}_{rot}^1, \mathbf{B}_{rot}^2, \dots, \mathbf{B}_{rot}^j, \dots, \mathbf{B}_{rot}^l]^T \end{aligned} \quad (10)$$

where l is the modal order. The elements of each row in the matrix can be calculated as follows

$$\begin{aligned} \mathbf{B}_{tran}^j &= \sum_{k=1}^n m_k \begin{bmatrix} u_{kx}^j \\ u_{ky}^j \\ u_{kz}^j \end{bmatrix} \\ \mathbf{B}_{rot}^j &= \sum_{k=1}^n m_k \begin{bmatrix} 0 & -r_{kz} & r_{ky} \\ r_{kz} & 0 & -r_{kx} \\ -r_{ky} & r_{kx} & 0 \end{bmatrix} \begin{bmatrix} u_{kx}^j \\ u_{ky}^j \\ u_{kz}^j \end{bmatrix} \end{aligned} \quad (11)$$

where n is the total number of elements after the flexible structure is dispersed, m_k is the mass of the k^{th} element, u_k is the displacement of the centroid of the k^{th} element, r_k is the position of the centroid of the k^{th} element, and the subscripts x , y , and z represent the direction of the coordinate [25].

By ignoring the influence of any one of attachments, liquid-filled tanks, and manipulators, or defining different modal orders, more models of different granularities can be obtained in the field model.

2) MULTI-PHYSICAL COUPLING MODEL IN CELESTIAL-SCALE

For the thermal subsystem, the coupling model of celestial-scale mainly consists of solar radiation, earth infrared radiation, earth reflection heat flow model. The formula is shown as follows

$$q_S^i = \alpha_{Si} S \phi_{1i} A_i, \quad q_E^i = \varepsilon_{ei} E_e \phi_{3i} A_i, \quad q_{ER}^i = \alpha_{Si} E_r \phi_{2i} A_i \quad (12)$$

where q_S^i is the solar radiation heat of node i , α_{Si} is the solar absorptivity of the outer surface of the satellite, S is the solar constant, A_i is the surface area of node i , ϕ_{1i} is the solar direct radiation angle coefficient of node i , q_E^i is the earth infrared radiation heat of node i , ε_{ei} is the emissivity of the outer surface of node i , E_e is the average infrared radiation density of the earth, and ϕ_{3i} is the earth infrared radiation angle coefficient of node i , q_{ER}^i is the earth reflection heat of node i , E_r is the average reflection density of the earth surface to solar radiation, ϕ_{2i} is the earth albedo coefficient of node i [24].

The main coupling of the model is that ϕ_{3i} , ϕ_{2i} and ϕ_{1i} are coupled with dynamics. Their formulas are related to some variables in dynamics, including orbital altitude, satellite attitude, sun vector, and earth vector [24].

3) MULTI-PHYSICAL COUPLING MODEL IN SATELLITE-SCALE

For the thermal subsystem, the coupling model of satellite-scale is mainly the satellite heat balance differential equation. The finite elements are meshed according to the satellite configuration, and models of different granularities can be subdivided according to the size of the finite element space. The equation is established as follows

$$\begin{aligned} T_i(t + \Delta t) &= T_i(t) + \Delta t (q_S^i(t) + q_E^i(t) + q_{ER}^i(t) + q_{Rad}^i(t) \\ &\quad + q_{Cond}^i(t) + P_i(t) - q_{OS}^i(t) - q_{IS}^i(t)) / (m_i c_i) \\ T_i(t_0) &= T_i^0 \end{aligned} \quad (13)$$

where T_i is the temperature of node i , t is the current time, Δt is the time interval, and t_0 is the initial time, m_i is the mass of node i , c_i is the specific heat capacity of node i , q_{Rad}^i is the total radiation heat, q_{Cond}^i is the total conduction heat, P_i is the sum of the thermal power of all working components belonging to node i , q_{OS}^i is the external surface heat dissipation, q_{IS}^i is the internal surface heat dissipation, T_i^0 is the initial temperature of node i [24].

The formula for calculating the heat radiation and conduction from other heat nodes is

$$q_{Rad}^i = \sum_{j=1}^N B_{j,i} A_j \varepsilon_j \sigma T_j^4, \quad q_{Cond}^i = \sum_{j=1}^N K_{j,i} (T_j - T_i) \quad (14)$$

where N is the total number of heat nodes, $B_{j,i}$ is the absorption factor of node i to node j , ε_j is the emissivity of node j , $K_{j,i}$ is the conduction factor between node j and node i [24].

The calculation formula for heat dissipation of the inner and outer surfaces is

$$q_{OS}^i = A_i \varepsilon_{ei} \sigma T_i^4, \quad q_{IS}^i = A_i \varepsilon_{ii} \sigma T_i^4 \quad (15)$$

where ε_{ei} is the emissivity of the outer surface, ε_{ii} is the inner surface of node i [24].

The main coupling of the model is that the internal thermal power of the nodes is coupled with other subsystems such as power supply, the formula for internal thermal power is

$$P_i = \sum_{k=1}^{N_i} f_{PTermal}(\mathbf{X}_{D_{i,k}}) \quad (16)$$

where N_i is the total number of all components of node i , $\mathbf{X}_{D_{i,k}}$ is the working state of the component, and its relational function with thermal power is $f_{PTermal}$.

4) MULTI-PHYSICAL COUPLING MODEL IN COMPONENT-SCALE

The coupling model of components in the thermal field and other physical fields is introduced by taking laser gyroscope and flywheel as examples. The laser gyroscope model contains the coupling relation with thermal field and radiation field, and it is formulated as

$$\omega_m = \frac{\lambda L_{laser} \Delta f_m}{4 A_{laser} n_r} \quad (17)$$

where ω_m is the measured value of satellite angular velocity, Δf_m is the measured value of the frequency difference between the positive and negative beams, λ is the wavelength of the light source, n_r is the normalized refractive index of the optical path, A_{laser} and L_{laser} are the area and perimeter surrounded by the closed optical path, respectively [26]. Δf_m can be calculated by the following formula

$$\Delta f_m = \Delta f_{real} + B_0 + B_1 + B_2 \quad (18)$$

where Δf_{real} is the real value of the frequency difference, B_0 is the error considers the zero-deviation error, B_1 is the random walk error caused by mechanical vibration used to suppressing the lock area, B_2 is the error caused by radiation flux accumulation [26]. B_0 is coupled with the temperature of thermal field calculation, B_2 is coupled with the space radiation field. The error model can be concluded as

$$\begin{aligned} B_0 &= a_0 + a_1 T_{laser} + a_2 T_{laser}^2 \\ B_1 &= \Omega_L \sqrt{S_K / (2\pi \Omega_{Dm})} \\ B_2 &= f_{Rad_RLG}(J (\geq E_0)) \end{aligned} \quad (19)$$

where a_0 , a_1 , and a_2 are the zero bias compensation coefficients obtained by fitting the measurement data, T_{laser} is the gyro temperature, Ω_L is the lock zone threshold, Ω_{Dm} is the peak jitter rate, S_K is the laser gyro scale factor [26], $J (\geq E_0)$ is the radiation flux of the gyro, f_{Rad_RLG} is the relational function between error and radiation flux [27].

The flywheel model includes the coupling relationship with thermal field and electric field which is given as

$$\begin{aligned} K_f &= \frac{\Delta T \times C_o \times \rho \times G}{1.047 \times 10^{-1} \times D_w \times \omega_w} \\ M_M &= K_M V_C \end{aligned} \quad (20)$$

where M_M is the motor output torque, K_M is the torque voltage ratio coefficient, V_C is the input voltage, K_f is the friction coefficient, C_o is the specific heat of the lubricating oil, ρ is the lubricating oil density, G is the oil required for circulating lubricating oil, D_w is the flywheel bearing diameter, ω_w is the rotor speed. Considering the friction factor, M_{f0} is the static friction torque of the bearing, the installation unit vector of the wheel in the satellite is \mathbf{r} [28]. The output torque of the wheels in the body coordinate is

$$\mathbf{M}_{wheel} = (M_M - M_{f0} - K_f \omega_w) \mathbf{r} \quad (21)$$

The ideal gyro model can be obtained without considering all the error terms, and the laser gyro models with different granularities can be obtained by ignoring some of the error terms. The ideal flywheel model is obtained without considering the friction factor. Considering constant friction and considering the coupling of friction and temperature, two finer granularity models are obtained.

IV. MULTI-GRANULARITY GENETIC PROGRAMMING OPTIMIZATION METHOD

According to the definition of satellite granularities in section II, there are three different granularity expressions for the satellite scheme **S**. In the GP method, tree structures of satellite schemes with different granularities are established in the following subsection A. In traditional GP, all individual models are of the same granularity, whereas in MGGPO, individual models of different granularities are included. How to replicate, crossover, mutate, and switch the granularity of individuals in a multi-granularity population is introduced in subsection B. Different granularity models have different uncertainties and computing resource requirements. How to adjust the proportion of population granularity to minimize the risk of problem-solving is introduced in subsection C.

A. MULTI-GRANULARITY TREE STRUCTURE

The five-level tree structure is used to describe the satellite system scheme [21]. In this paper, combined with the definition of the multi-granularity model, each node of the tree structure is redefined, and the tree structures of the point model, stream model, and field model are obtained.

1) POINT MODEL TREE STRUCTURE

The tree structure of the point model of the satellite system scheme is shown in Fig. 1.

The level 1 nodes in Fig. 1 represent different satellite schemes described by the point model. There are two kinds of granularity of subsystem nodes. One is the ideal subsystem node, and the other is the real subsystem node. In the 2nd level nodes, the nodes of the payload subsystem are real subsystem nodes, and the nodes of other subsystems are defined as ideal subsystem nodes, such as the ‘‘IdealADCS’’ nodes in Fig 1. Only the 3rd level nodes of the payload subsystem indicate device categories, such as infrared payload, optical payload, and SAR. The 3rd level nodes of the remaining

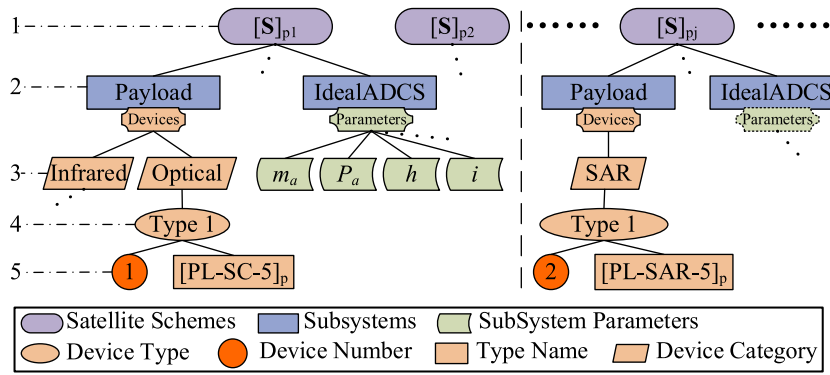


FIGURE 1. Point model tree structure of satellite system schemes.

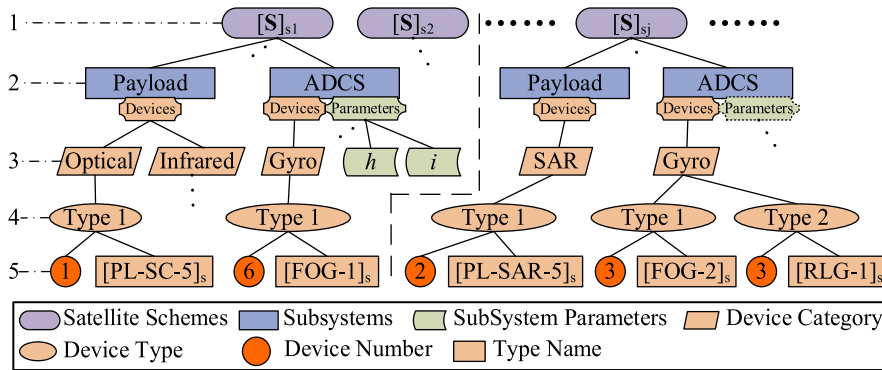


FIGURE 2. Stream model tree structure of satellite system schemes.

subsystems are subsystem parameter nodes, as ADCS subsystem mass (m_a), electric power (P_a), orbital altitude (h), and inclination (i) shown in Fig.1. In the 5th level nodes, each “Type Name” node corresponds to a point granularity component model of that type. For example, “[PL-SC-5]_p” represents a point granularity model of a type of optical payload component named “PL-SC-5”.

2) STREAM MODEL TREE STRUCTURE

The tree structure of the stream model of the satellite system scheme is shown in Fig. 2.

The level 1 nodes in Fig. 2 represent different satellite schemes described by the stream model. In the 2nd level nodes, all the nodes are real subsystem nodes, such as the “Payload” and “ADCS” nodes in Fig 2. The 3rd level nodes of each subsystem may contain two kinds of branches, namely “Device Category” nodes and “Subsystem Parameters” nodes. In the 5th level nodes, each “Type Name” node corresponds to a stream granularity component model of that type. For example, “[PL-SAR-5]_s” represents a stream granularity model of a type of SAR payload component named “PL-SAR-5”.

3) FIELD MODEL TREE STRUCTURE

The tree structure of the field model of the satellite system scheme is shown in Fig. 3.

The 1st level nodes in Fig. 3 represent different satellite schemes described by the field model. In the 2nd level nodes, all the nodes are real subsystem nodes. The 3rd level nodes of each subsystem may contain three kinds of branches, namely “Device Category” nodes, “Subsystem Parameters” nodes, and “Dynamics” nodes. The “Dynamics” nodes represent the coupling model of multi-dynamic and multi-physical fields contained in the subsystem. For example, “Flexible Wing” represents the flexible solar wing model, and “Manipulator” represents the manipulator model. In the 5th level nodes, each “Type Name” node corresponds to a field granularity component model of that type. For example, “[FOG-1]_f” represents a field granularity model of a type of fiber optic gyroscope named “FOG-1”.

B. MULTI-GRANULARITY GENETIC PROGRAMMING OPERATION

As shown in Fig. 3, nodes of the parse tree are divided into two categories. One category is called “operator”, which locates in the internal of the tree. The other category is called “terminator” located in the terminal of the tree. The definitions of operator set and terminator set are shown in Table 1.

The basic operations of GP include replication, crossover, and mutation. In this paper, the genetic operation among individuals of the same granularity in the population is consistent with the method in [21]. A method of how to deal

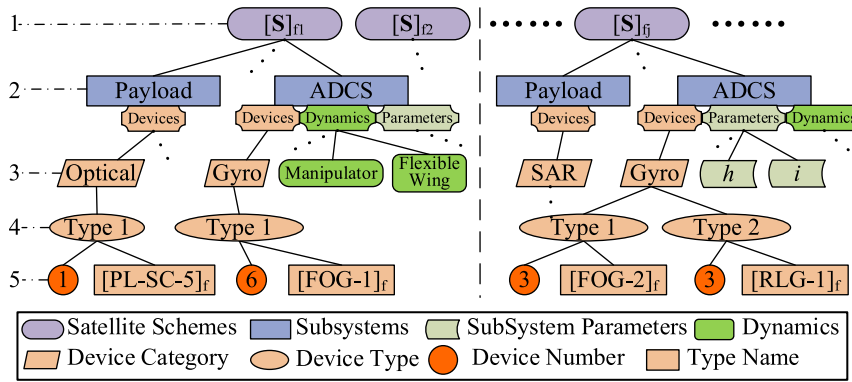


FIGURE 3. Field model tree structure of satellite system schemes.

TABLE 1. Definition of operator set and terminator set.

Node category	Node Symbol	Corresponding nodes in the tree structure
operator set	"Satellite"	the 1st level nodes of the tree structure
	"Subsystem"	the subsystem nodes in the 2 nd level
	"Parameters"	the subsystem parameter branch nodes in the 2 nd level
	"Devices"	the devices branch nodes in the 2 nd level
	"Dynamics"	the dynamics branch nodes in the 2 nd level
	"DeviceCategory"	the device category nodes in the 3 rd level
	"DeviceType"	the device type nodes in the 4 th level
terminator set	"Name"	the device type name nodes in 5 th level
	"NUM"	the device number nodes in 5 th level
	"ParaInfo"	the parameter information nodes in the 3 rd level
	"DynamicInfo"	the dynamic information nodes in the 3 rd level

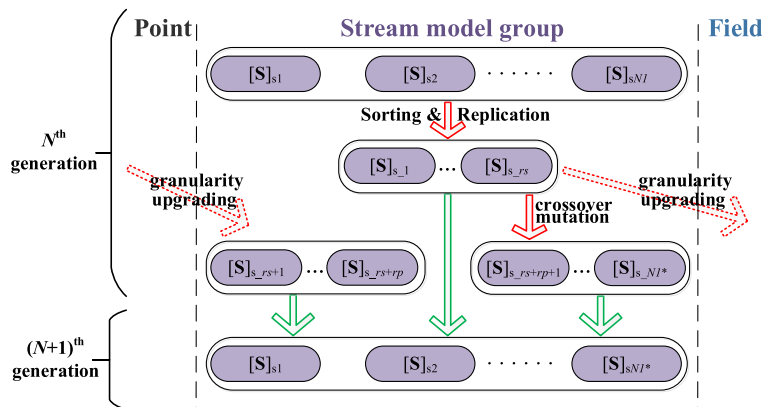


FIGURE 4. Schematic diagram of population multi-granularity GP operations.

with the relationship between groups of individuals with different granularities in a population is proposed. The sorting, replication, crossover, and mutation operations of population individuals have all been modified. In the sorting operation, the individuals in different granularity groups are compared separately and sorted in each group according to the fitness. In the replication operation, the number of individuals to be replicated in the group is obtained by multiplying the total number of individuals in the group by the replication proportion. Several individuals with high fitness are replicated from different granularity groups to join the next generation.

After the granularities of replicated individuals are upgraded, new individuals are generated to join the next generation. The remaining individuals are generated by crossover and mutation. Two individuals from each group of replicates are selected for crossover operations. The new individuals generated by crossover are mutated according to the set probability. The resulting new individuals are added to the next generation. The individual group of the stream model is taken as an example. The process of generating the $(N + 1)^{th}$ generation individuals through multi-granularity GP operations is shown in Fig. 4.

In Fig. 4, NI is the total number of individuals in the stream model group of N^{th} generation, NI^* is the one of $(N + 1)^{\text{th}}$ generation. “ rs ” represents the number of individuals to be replicated in the stream model group, “ rp ” is the one of the point model group. $[S]_{s\%}$ represents the individuals in the next generation population generated by various operations, where the subscript at the “ $\%$ ” position indicates the index of individuals.

C. DEFINITION OF RISK FACTOR AND OPTIMIZATION OF POPULATION SIZE PROPORTION

The risk caused by model uncertainty and simulation time consumption is considered. If all the individuals in the population are point models, the uncertainty of the model is large, in which case the optimal solution may not be obtained and the risk is high. If all of them are field models, they may not be able to converge in finite time under urgent tasks, and the risk is high as well. Theoretically, mixing different granularities in a reasonable proportion can minimize the risk. The risk factor can be defined as follows

$$K_{risk} = \mu_{point}P_{point} + \mu_{stream}P_{stream} + \mu_{field}P_{field} + |\mu_{time}(T_{generation} - T_{expected})| \quad (22)$$

where K_{risk} is the risk factors of population, μ_{point} , μ_{stream} , μ_{field} represent the uncertainty of the point model, stream model, and field model respectively, P_{point} , P_{stream} , P_{field} represent the proportion of point model, flow model and field model in the population respectively, μ_{time} is the risk coefficient of simulation time consumption, $T_{generation}$ represents the total simulation time required to complete the evaluation of all schemes of a certain generation, $T_{expected}$ represents the expected time for each generation to complete the optimization on time.

Based on the risk factor, the proportion of granularity diversification is adjusted to the direction of low risk in the process of satellite scheme optimization. After the simulation of each generation of population, according to the previous simulation history data, the average simulation time of each granularity individual is calculated. T_{avg_point} , T_{avg_stream} , T_{avg_field} are the average simulation time of the point model, stream model, and field model respectively. $N_{population}$ is the total number of individuals in a population, f_{Tgen} is the function to predict the total simulation time of the next generation $T_{generation}$ according to the population size, granularity proportion, and average simulation time. $T_{generation}$ can be expressed as follows

$$T_{generation} = f_{Tgen}(N_{population}, P_{point}, P_{stream}, P_{field}, T_{avg_point}, T_{avg_stream}, T_{avg_field}) \quad (23)$$

The proportion of each granularity P_{point} , P_{stream} , P_{field} are taken as the design variables. The risk factor K_{risk} is defined as the objective function. The relationship between each proportion and $T_{generation}$ is set as the constraints. The optimization model of granularity proportion is

established as follows

$$\begin{aligned} \text{find} \quad & P_{point} \in [P_{point_min}, 1] \\ & P_{stream} \in [P_{stream_min}, 1] \\ & P_{field} \in [P_{field_min}, 1] \\ \text{min} \quad & K_{risk} \\ \text{s.t.} \quad & P_{point} + P_{stream} + P_{field} = 1 \\ & T_{generation} \leq T_{expected} \end{aligned} \quad (24)$$

where P_{point_min} , P_{stream_min} , and P_{field_min} are the minimum proportions of the point model, stream model, and field model in the population.

V. FLOWCHART OF SATELLITE SYSTEM DESIGN OPTIMIZATION BASED ON MGGPO

The optimization framework is shown in Fig. 5, which includes a two-level optimization iterative process, that is, the optimization of the satellite scheme and the optimization of the population granularity proportion in each generation. The optimization process of the satellite scheme is divided into two modules: GP, Modeling & Evaluation.

The optimization process starts with the GP module. The 1st step is to initialize the GP parameters. In the 2nd step, the initial multi-granularity satellite scheme population is generated with the initial population granularity proportion, and the multi-granularity tree structure of the satellite individuals is obtained. In the 3rd step, the multi-granularity tree structure is transformed into the multi-granularity satellite scheme description based on the component library. Then the optimization process gets into the Modeling & Evaluation module. In the 4th step, for each individual in the population, the satellite digital model with corresponding granularity is established, and the satellite evaluation condition set is designed from the condition library. In the 5th step, the batch processing method is used to complete the calculation in the verification simulation condition set. In the 6th step, the evaluation index of each scheme in the population is obtained by statistics of the simulation results of the condition set. In the 7th step, the fitness value is calculated according to the evaluation indices. After the 7th step, the optimization process enters two branches, one is to the granularity proportion optimization, and the other is to the GP module. In the 8th step, after the simulation of all the schemes of the current generation population is completed, the average simulation time of each granularity is evaluated, and the initial population of granularity proportion for the granularity proportion optimization is generated based on the granularity proportion of the current generation. In the 9th step, according to the simulation time and the uncertainty of the model, the risk factors corresponding to all granularity proportions in the population of granularity proportions are calculated. In the 10th step, the granularity proportions are ranked according to their risk factors. The 11th step is to judge whether the minimum risk factor is smaller than the expected value. If so, stop the granularity proportion optimization, and the optimal granularity

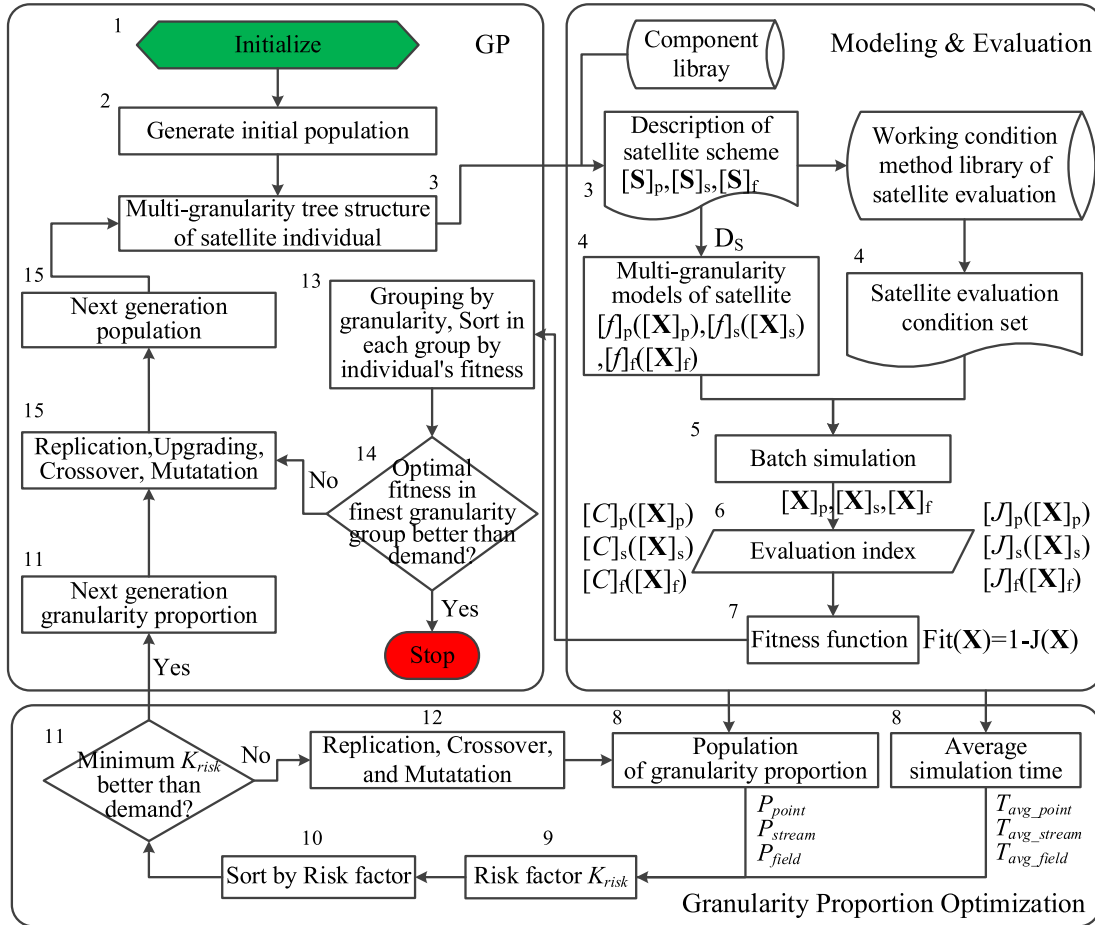


FIGURE 5. Flowchart of two-level optimization of the satellite scheme (system topology and parameter) and the population granularity proportion. The component library consists of all component models that can support the satellite system design [29], [30]. $Fit(\mathbf{X})$ is the fitness function.

proportion is returned to the GP module as the granularity proportion of the next-generation satellite scheme population. If not, the process enters the 12th step, a new population of granularity proportion is generated by the genetic operation of replication, crossover, and mutation. Then continue to loop from the 9th step to the 12th step until the termination condition is met. In the 13th step, the optimization process returns to the GP module, and individuals in the population are grouped by their granularity and ranked in each group according to their fitness. The 14th step is to judge whether the optimal fitness in the finest granularity group is better than the expected value. If so, stop the optimization to get the optimal result. If not, the process enters the 15th step, the next-generation population of design schemes is generated by the genetic operation of replication, upgrading, crossover, and mutation, in which the granularity proportion obtained from the 8th step to the 12th step is used. The multi-granularity individual tree structure of the next-generation population is looped from the 3rd step to the 15th step until the termination conditions are satisfied, and the ideal satellite design results are obtained.

VI. APPLICATION OF MGGPO INTO AN EARTH OBSERVATION SATELLITE

The earth observation satellite described in [31] is taken as an instance. The ADCS, power, thermal, TT&C, propulsion, payload, and structure subsystems are selected to optimize the system composition, structure, and parameters. The weighted coefficients of the main optimization objectives are set as [21]. The optimizer parameters are set as Table 2 in which parameters for the optimization of the satellite system scheme are set according to [21].

The multi-granularity tree structure of the satellite scheme is taken as the design variable. It mainly includes the parameters and composition of the satellite system and the parameters of the satellite subsystem. System composition includes component type selection and the number of components of each subsystem, and its screening scope is the component library described in Section V. System structure information refers to the multi-granularity models of subsystems, and its model construction and parameter selection are implemented according to Section III. The main constraints in the satellite subsystem parameter

TABLE 2. Optimizer parameters.

Type	Parameter Name	Value
Optimization of satellite system scheme	The number of individuals in each generation	10
	The maximum number of iterations	100
	The number of individuals performing the replication operation	2
	The probability of crossover	0.5
	The probability of mutation	0.2
Optimization of granularity proportion	The minimum fitness for the termination condition	0.9
	The initial proportion of the point model	0.4
	The initial proportion of the stream model	0.5
	The initial proportion of the field model	0.1
	The minimum value of the proportion of the point model	0.1
	The minimum value of the proportion of the stream model	0.1
	The minimum value of the proportion of the field model	0.1
	The uncertainty of the point model	4
	The uncertainty of the stream model	2
	The uncertainty of the field model	1
	The expected total simulation time / d	15
	The number of the granularity proportion individuals	100
	The number of individuals performing the replication operation	20
	The probability of crossover	0.5
	The probability of mutation	0.3
The maximum risk factor for the termination condition	10	

TABLE 3. Subsystem level constraints.

Subsystem	Parameter Name	Symbol	Bounds
ADCS	Attitude measurement accuracy requirements / °	$\delta_{measure}$	≤ 0.001
	Attitude pointing accuracy requirements / °	δ_{point}	≤ 0.001
	Attitude stability accuracy requirements / °/s	δ_{stable}	≤ 0.001
	Attitude maneuver angular velocity requirements / °/s	$\omega_{maneuver}$	≥ 0.01
	Orbit control accuracy requirements / m	δ_{orbit}	≤ 1
	Minimum orbit control acceleration / m/s ²	a_{oc}	≥ 0.05
Payload	Minimum coverage bandwidth / m	S_w	≥ 50000
	Minimum image SNR / db	SNR	≥ 50
Power	Maximum discharge depth / %	DOD	≤ 35
	Average eclipse factor	k_e	≤ 0.9
Propulsion	Propellant extrusion efficiency	EOP	≥ 0.9
TT&C	Minimum quality requirement / db	GT	≥ 0.1
	Minimum requirement ERIP / dbw	$ERIP$	$\geq 1.0e-6$
Thermal	Satellite equilibrium temperature / °C	T_{bal}	0-50
	Satellite temperature range / °C	T_i	0-50
Structure	Axial frequency / Hz	f_{axi}	≥ 24
	Lateral frequency / Hz	f_{lat}	≥ 10
	Effective space diameter of fairing / m	d_b	≤ 3.5
	Effective space height of fairing / m	h_b	≤ 6
	Satellite volume / m ³	V_{sat}	≥ 1
	Structural reliability factor	$Index_{str}$	≥ 1

information are consistent with those in [21], as shown in Table 3.

The ranges, initial values of system-level design variables are consistent with those in [21]. The optimization result of traditional GP in [21] is given in the 5th column of Table 4. The optimization result of the MGGPO method proposed in this paper is given in the 6th column of Table 4, and the change percentage is given in the last column of Table 4. Compared with the results of GP, the results of MGGPO have three significant differences, including a 16.73% reduction in the total mass of the satellite, a 40% reduction in the shell thickness, and a 53.88% reduction in the design life within the design ranges. The other results are similar, less than 10%.

The optimization results of system composition and parameters are shown in Table 5. By comparing the optimized schemes of GP and MGGPO, we can see that the system

composition has significantly changed. The main changes are the type and number of components. It can also be seen from Table 5 that the parameters of components vary with the component models. To sum up, the results show that the MGGPO method in this paper is feasible to realize the simultaneous optimization of satellite system topology and parameters.

The change of the optimal fitness value of each generation in GP and MGGPO is compared in Fig. 6(a). The results show that the MGGPO algorithm shows good convergence, and the convergence trend of the results is consistent with GP. The optimal fitness of the two methods is almost the same, and the final difference is 2.1%. The optimization results of performance, quality, cost, reliability, and cost-effectiveness ratio are normalized, and the larger the value, the better the result. As shown in Fig. 6(b), the results of MGGPO and

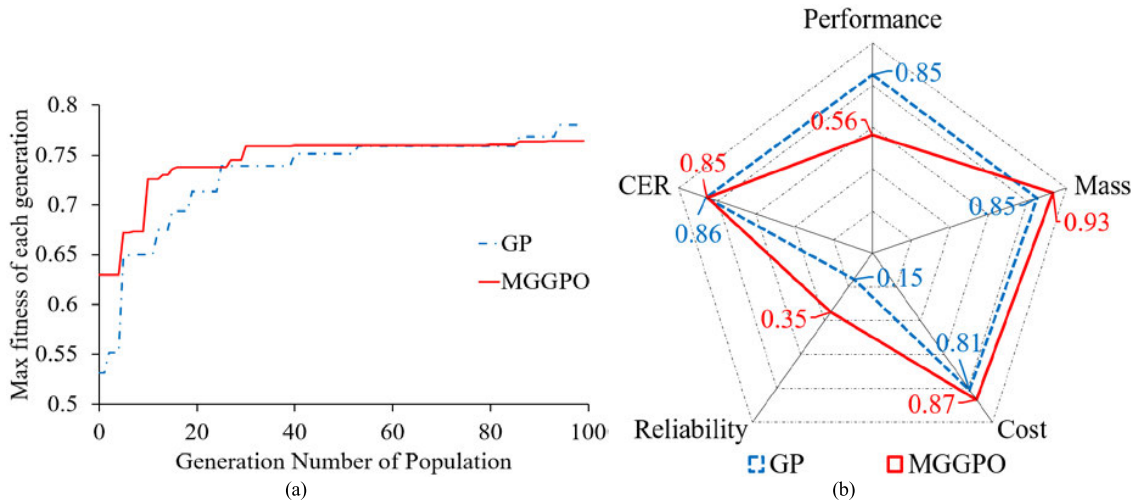


FIGURE 6. GP and MGGPO optimization results of fitness and system indexes. (a) Relationship between optimal fitness value and generation number of population, (b) Optimization results of normalization system indexes.

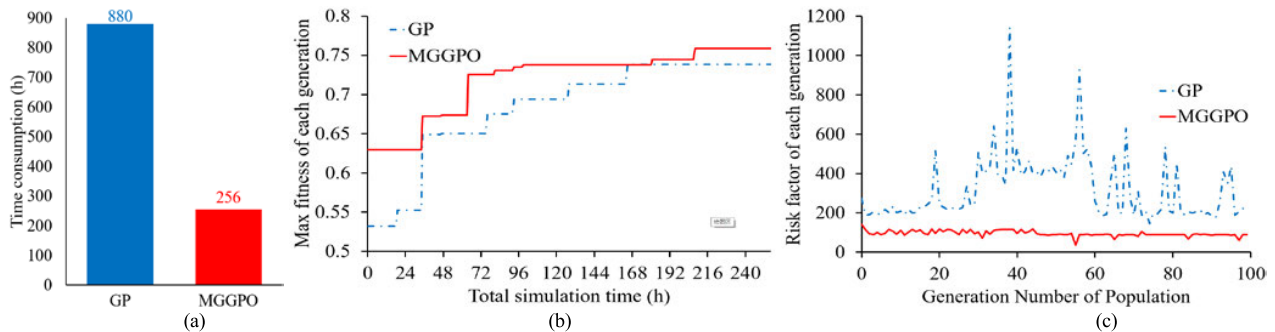


FIGURE 7. Performance comparison with traditional GP optimization tools. (a) The comparison of total simulation time (b) The comparison of fitness changing with time, (c) The comparison of risk factors changing with the generation number of population under the same expected time.

GP methods have a small difference of about 1.2% in the cost-effectiveness index (CER). In the results, the performance index optimized by GP is better. However, the quality, cost, and reliability indices optimized by MGGPO are better.

Table 4 and Fig. 6(a) show that MGGPO methods can be used to obtain traditional system parameter optimization results. Table 5 shows that the MGGPO method is used to optimize the composition and structure of the satellite system, which is difficult to be realized by traditional algorithms such as GA in [31]. The above results substantiate the effectiveness of the proposed MGGPO method.

The design and optimization of the Earth Observation Satellite by both GP and MGGPO methods are established under the same hardware and software environment. Detailed implementation details are listed in Table 6.

To compare the optimization performance, we perform a 100-generation optimization procedure by taking both methods. As shown in Fig. 7(a), MGGPO takes 256 hours to finish the optimization, which is 71% shorter than that of GP (880 hours). Fig. 7(b) shows that MGGPO converges faster and the optimization result is better than GP under the same time consumption. Fig. 7(c) indicates that the average risk factor value of MGGPO is 70% smaller, the maximum value is 39% smaller, and the minimum value is 94% smaller than those of GP, respectively.

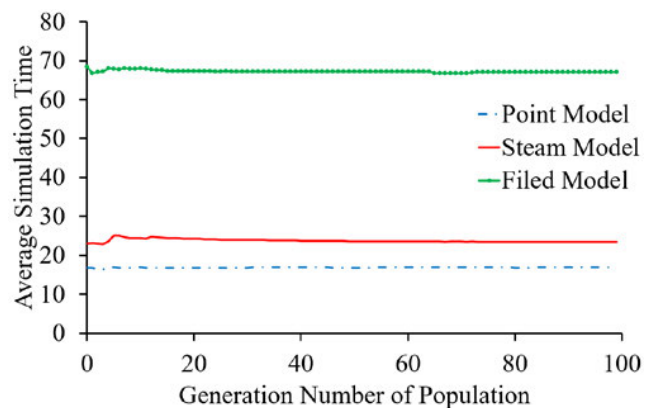


FIGURE 8. GP and MGGPO optimization results of fitness and system indexes.

To quantitatively compare the computational complexity of different granularity models, we calculate the average simulation time of each generation of different granularity schemes in the above cases, as shown in Fig. 8.

It can be seen from Fig. 8 that the computational complexity of the point model is the lowest, while that of the stream model is 38.9% higher than that of the point model, while that of the field model is the highest, which is about 3.98 times of that of the point model.

TABLE 4. Optimization results of GP And MGGPO on system-level design variables.

Subsystem	Parameter Name	Symbol	Ranges	Result (GP)	Result (MGGPO)	Changes (%)
ADCS	Orbital height / km	h	[600,1000]	736.1	767.3	4.24
	Orbit inclination / °	i	[95,105]	100.4	96.19	-4.19
Power	Local time of descending node / h	d_{nt}	[8,12]	10	9	-10
	Life / a	L_{ife}	[3,10]	6.614	3.050201	-53.88
Structure	Total mass of the satellite / kg	m	[500,2000]	726.2	604.7	-16.73
	Envelope diameter / m	d_b	[0.4,4]	1.414	1.414	0.00
	Shell thickness / m	t_s	[0.005,0.5]	0.01	0.006	-40.00
	Envelope height / m	h_b	[0.5,6]	1	1	0.00
	Material type	$Material$	{1,2,3,4}	2	2	/
	Safety factor	$Index_{min}$	[1,1.1]	1.078	1	-7.24
	Bearing cylinder diameter /m	$d_{cylinder}$	[0.1,2]	0.2367	0.25	5.62

TABLE 5. Optimization results of GP and MGGPO on key components in the tree structure.

Component category	GP optimized scheme			MGGPO optimized scheme		
	Type	Num.	Para.	Type	Num.	Para.
Camera	PL-SC-5m-50	1	focal length 100 mm	PL-SC-5m-50	1	focal length 100 mm
			View angle 30°			View angle 30°
			Pixel size 10 μm			Pixel size 10 μm
Flywheel	MW-2Nm	5	Angular Momentum 1.88 N·m·s	MW-1Nm	4	Angular Momentum 0.957 N·m·s
Solar Wing	GaAs-18	2	Area 10.39 m ²	GaAs-20	2	Area 8.88 m ²
Thruster	TH-2N	8	Force 0.1 N	TH-1N	7	Force 0.1 N
Antenna	AT-L1500	1	Area 1.5 m ²	AT-L1000	1	Area 1.0 m ²
Hot Window	HW-R088	2	Area 0.3229 m ²	HW-R086	2	Area 0.3158 m ²

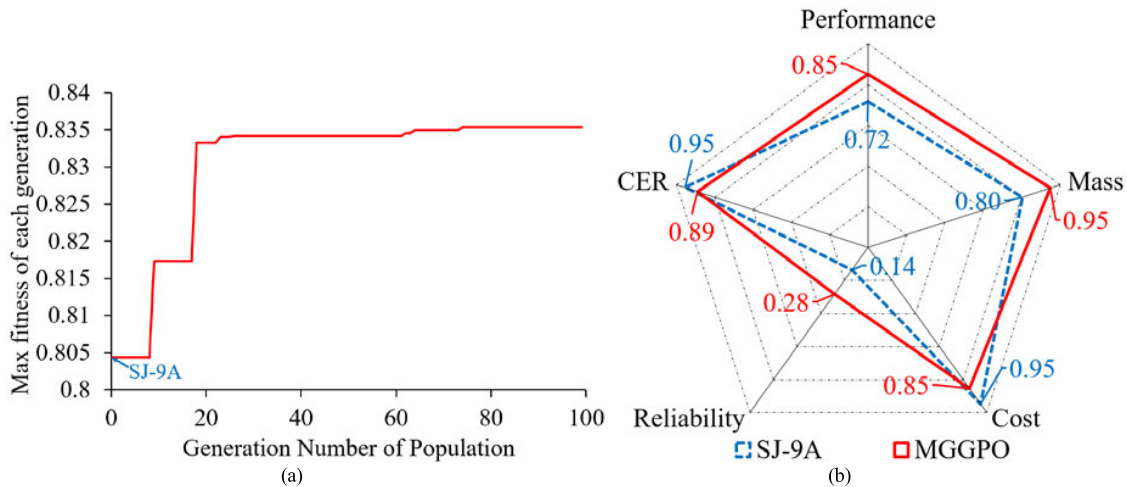


FIGURE 9. Comparison of MGGPO optimization results with SJ-9A satellite designed by traditional methods. (a) Relationship between optimal fitness value and generation number of population, (b) Comparison of normalization system indexes.

TABLE 6. Hardware and software environment.

Environment	Category	Details
Hardware	Total Number of physical cores	126
	Frequency of each physical core	3.2G Hz
Software	Operating system	Win10
	Development and runtime	C/C++, C#, MATLAB

To compare with the traditional satellite design optimization method, the design scheme of the SJ-9A satellite is selected as the reference group. SJ-9A satellite is an experimental satellite launched by China in 2012. It is a typical satellite designed by traditional satellite design optimization methods. The design scheme of the SJ-9A satellite is added to the initial population of optimization. Under the

same evaluation system, better results are obtained after 100 generations of optimization iterations. Fig. 9(a) shows the convergence process of fitness, and the final optimized fitness is 3.9% higher than that of the SJ-9A satellite. Fig. 9(b) shows the comparison of the main indices. It can be seen that the SJ-9A satellite is better for the two indices of total cost and cost-effectiveness ratio, while MGGPO is better for the other three indices.

VII. CONCLUSION

In this paper, an MGGPO method for satellite system topology and parameter design and optimization is proposed aiming to reduce the consumption of optimization resources as well as to reduce the convergence time. The optimization

results show that the MGGPO method can simultaneously optimize satellite system parameters, composition, and structure by taking an earth observation satellite as an instance. MGGPO is 71% faster than traditional GP with only a 2.1% loss in fitness. In the comparison with the SJ-9A satellite, the fitness was improved by 3.9% after optimization of MGGPO. The construction method of the multi-granularity model and the optimization method of multi-granularity genetic programming can be extended to the system design of other spacecraft. In this paper, the uncertainties of different granularity models are defined based on experience, which may not be the most reasonable values. The quantitative evaluation of the uncertainty of model granularity can be further studied. Similarly, the definition of the risk factor is also based on experience. The impact of different risk factor definition models on optimization performance and results can be further studied.

REFERENCES

- [1] W. P. Rogers, "Report of the presidential commission on the space shuttle challenger accident," Appendix F, US Government Printing Office, Washington, DC, USA, Tech. Rep. 12546, Feb. 1986.
- [2] J. K. Esser and J. S. Lindofer, "Groupthink and the space shuttle challenger accident: Toward a quantitative case analysis," *J. Behav. Decis. Making*, vol. 2, no. 3, pp. 167–177, Jul. 1989.
- [3] J. L. Hall, "Columbia and challenger: Organizational failure at NASA," *Space Policy*, vol. 19, no. 4, pp. 239–247, Nov. 2003.
- [4] M. Conroy, R. Mazzone, and W. Lin, "NASA integrated model-centric architecture (NIMA) model use and re-use," in *Proc. IEEE Aerosp. Conf.*, Mar. 2013, pp. 1–15.
- [5] S. C. Spangelo, J. Cutler, L. Anderson, E. Fosse, L. Cheng, R. Yntema, M. Bajaj, C. Delp, B. Cole, G. Soremekum, and D. Kaslow, "Model based systems engineering (MBSE) applied to radio aurora explorer (RAX) CubeSat mission operational scenarios," in *Proc. IEEE Aerosp. Conf.*, Mar. 2013, pp. 1–18.
- [6] G. Cataldo, M. B. Niedner, D. J. Fixsen, and S. H. Moseley, "Model-based thermal system design optimization for the James Webb space telescope," *J. Astronomical Telescopes Instrum. Syst.*, vol. 3, no. 4, pp. 44001–44002, 2017, doi: [10.1117/1.JATIS.3.4.044002](https://doi.org/10.1117/1.JATIS.3.4.044002).
- [7] E. Fosse, A. Devereaux, C. Harmon, and M. Lefland, "Inheriting curiosity: Leveraging MBSE to build Mars2020," in *Proc. AIAA SPACE Conf. Expo.* Reston, VA, USA: American Institute of Aeronautics and Astronautics, Aug. 2015, p. 4617.
- [8] H. A. Saleh and R. Chelouah, "The design of the global navigation satellite system surveying networks using genetic algorithms," *Eng. Appl. Artif. Intell.*, vol. 17, no. 1, pp. 111–122, Feb. 2004, doi: [10.1016/j.engappai.2003.11.001](https://doi.org/10.1016/j.engappai.2003.11.001).
- [9] Q. He and C. Han, "Satellite constellation design with adaptively continuous ant system algorithm," *Chin. J. Aeronaut.*, vol. 20, no. 4, pp. 297–303, Aug. 2007.
- [10] C. D. Jilla and D. W. Miller, "Assessing the performance of a heuristic simulated annealing algorithm for the design of distributed satellite systems," *Acta Astronautica*, vol. 48, no. 5, pp. 529–543, 2001, doi: [10.1016/S0094-5765\(01\)00057-1](https://doi.org/10.1016/S0094-5765(01)00057-1).
- [11] J. Koza, *Genetic Programming: On the Programming of Computers by Means of Natural Selection*. Cambridge, MA, USA: MIT Press, 1992.
- [12] T. Sripramong and C. Toumazou, "The invention of CMOS amplifiers using genetic programming and current-flow analysis," *IEEE Trans. Comput.-Aided Design Integr. Circuits Syst.*, vol. 21, no. 11, pp. 1237–1252, Nov. 2002, doi: [10.1109/TCAD.2002.804109](https://doi.org/10.1109/TCAD.2002.804109).
- [13] G. J. Sun, J. H. Li, S. M. Chen, and Y. F. Dong, "The satellite attitude control law design based on machine learning," *Appl. Mech. Mater.*, vols. 519–520, pp. 741–746, Feb. 2014, doi: [10.4028/www.scientific.net/AMM.519-520.741](https://doi.org/10.4028/www.scientific.net/AMM.519-520.741).
- [14] G. Malhotra, V. Lekshmi, S. Sudhakar, and S. Udupa, *Implementation of Threshold Comparator Using Cartesian Genetic Programming on Embryonic Fabric*. Cham, Switzerland: Springer, 2018, pp. 93–102.
- [15] Y. Chen, Z. Zhou, and G. Qu, "Application of multidisciplinary design optimization in satellite design," *Spacecraft Eng.*, vol. 22, no. 3, pp. 16–24, 2013.
- [16] B. Zhang and L. Zhang, *Theory and Applications of Problem Solving*. Amsterdam, The Netherlands: North-Holland, 1992.
- [17] L. Zhang and B. Zhang, "A quotient space approximation model of multiresolution signal analysis," *J. Comput. Sci. Technol.*, vol. 20, no. 1, pp. 90–94, Jan. 2005, doi: [10.1007/s11390-005-0010-8](https://doi.org/10.1007/s11390-005-0010-8).
- [18] L. Zhang and B. Zhang, "The structure analysis of fuzzy sets," *Int. J. Approx. Reasoning*, vol. 40, nos. 1–2, pp. 92–108, Jul. 2005, doi: [10.1016/j.ijar.2004.11.003](https://doi.org/10.1016/j.ijar.2004.11.003).
- [19] A. M. Madni and M. Sievers, "Model-based systems engineering: Motivation, current status, and research opportunities," *Syst. Eng.*, vol. 21, no. 3, pp. 172–190, May 2018, doi: [10.1002/sys.21438](https://doi.org/10.1002/sys.21438).
- [20] Y. Chen, M. Wang, and B. Liu, "Research progress of the integrated optimization design for the GEO spacecraft," *Astron. Syst. Eng. Technol.*, vol. 2, no. 3, pp. 18–24, 2018.
- [21] J. Li, Y. Dong, M. Xu, and H. Li, "Genetic programming method for satellite system topology and parameter optimization," *Int. J. Aerosp. Eng.*, vol. 2020, pp. 1–14, Dec. 2020, doi: [10.1155/2020/6673848](https://doi.org/10.1155/2020/6673848).
- [22] C. Zheng and L. Zhang, "The computation of maximum flow in network analysis based on quotient space theory," *Chin. J. Comput.*, vol. 38, no. 8, pp. 1705–1712, 2015, doi: [10.11897/SP.J.1016.2015.01705](https://doi.org/10.11897/SP.J.1016.2015.01705).
- [23] Y. Dong, S. Chen, J. Su, and D. Hu, *Dynamic Simulation Technology of Satellite Attitude Control*. Beijing, China: Science Press, 2010.
- [24] H. Li, *Satellite Thermal Control Technology*. Beijing, China: China Astronautical Publishing House, 2007.
- [25] X. Wei and Y. F. Dong, "Calculation of translational and rotational coupling coefficient matrix based on ANSYS," in *Proc. 21st Annu. Meeting Beijing Soc. Mech., 22nd Annu. Meeting Beijing Soc. Vib. Eng.*, 2015, p. 3.
- [26] Z. Hu, *Study on Error Model of the Ring Laser Gyro*. Xi'an, China: Northwest Univ., 2008.
- [27] H. Zhuang, R. Ma, Y. Wu, and S. Gu, *Aerospace Environment Manual*. Beijing, China: Space science and Application Research Center, Chinese Academy of Sciences, 2000.
- [28] G. Xuebing, W. Rixin, and X. Minqiang, "Abnormality detection for flywheels based on data association analysis," *Acta Astronautica Sinica*, vol. 36, no. 3, pp. 898–906, 2015, doi: [10.7527/S1000-6893.2014.0124](https://doi.org/10.7527/S1000-6893.2014.0124).
- [29] R. Min, D. Yunfeng, and L. Chang, "Code generation technology of digital satellite," in *Proc. Int. Conf. Extreme Learn. Mach.*, 2015, pp. 511–519.
- [30] H. Li and Y. Dong, "Intelligent development technology of satellite fault diagnosis system," *Aerospace Shanghai*, vol. 34, no. 3, pp. 52–59, 2017.
- [31] X. Wei, *Agent Negotiation Based Collaboration Optimization and Its Application to Satellite System Design*. Beijing, China: Beihang Univ., 2017.



JINHUI LI received the B.S. degree in engineering mechanics from the School of Mechatronic Engineering, Beijing Institute of Technology, China, in 2012. He is currently pursuing the Ph.D. degree in spacecraft design with the School of Astronautics, Beihang University, China. His research interests include spacecraft system design, system topology optimization, genetic programming, and construction of satellite digital twin systems.



YUNFENG DONG received the B.S., M.S., and Ph.D. degrees from the School of Astronautics, Beihang University, China, in 1987, 1990, and 2005, respectively. He is currently a Professor with the School of Astronautics, Beihang University. His research interests include spacecraft system design, spacecraft dynamics and control, application of artificial intelligence, model-based systems engineering, and digital twin in aerospace.